Reliability Engineering and System Safety 95 (2010) 632–646

Contents lists available at ScienceDirect

Reliability Engineering and System Safety

journal homepage: www.elsevier.com/locate/ress

Uncertainty quantification in simulations of power systems: Multi-element polynomial chaos methods

P. Prempraneerach [a], F.S. Hover [a], M.S. Triantafyllou [a], G.E. Karniadakis [a,b,*]

[a] Department of Mechanical Engineering, Massachusetts Institute of Technology, Cambridge, MA 02139, USA
[b] Division of Applied Mathematics, Brown University, 182 George Street, Box F, Providence, RI 02912, USA

ARTICLE INFO

Article history:
Received 3 August 2009
Received in revised form
25 January 2010
Accepted 26 January 2010
Available online 2 February 2010

Keywords:
Uncertainty analysis
Monte-Carlo simulation
Power systems

ABSTRACT

While probabilistic methods have been used extensively in simulating stationary power systems, there has not been a systematic effort in developing suitable algorithms for stochastic simulations of time-dependent and reconfiguring power systems. Here, we present several versions of polynomial chaos that lead to a very efficient approach especially in low dimensions. We consider both Galerkin and Collocation projections, and demonstrate how the multi-element decomposition of random space leads to effective resolution of stochastic discontinuous solutions. A comprehensive comparison is presented for prototype differential equations and for two electromechanical systems used in an electric ship.

1. Introduction

The advent of modern power electronics and large-scale power converters is ushering in a new age for electric ship-propulsion. This is embodied in the All-Electric Ship (AES) concept, where a set of prime movers is used to power all loads on the ship-propulsion, weaponry, HVAC, lighting, and other systems [1]. This paradigm has a number of well-known advantages relative to conventional ships, including reduced fuel usage, reduced maintenance, and increased design flexibility. An integrated power system (IPS) is required to effectively manage the many sensors, motors, relays, and processors that make up the system.

At the design stage, performance and robustness of candidate solutions are evaluated by studying system response to variations in loading conditions and in system parameters. For low-dimension systems having simple dynamic behavior, this can be achieved by deterministically varying a few parameters at a time. Exploring the space in a methodical or *ad hoc* manner, the designer hopes to gain insight into the system behavior, and may be able to uncover conditions of unacceptably high sensitivity. When many uncertainties exist or when the system response is more complex, the deterministic technique will be less successful, in part because complex simulations simply take longer to run, and because the matrix of coincident parameters to vary grows exponentially with the number of random dimensions. For these cases, a stochastic approach is more appropriate; the uncertainties are assumed to take a specific distribution, and the outcome of the calculation is a statistical description of the system behavior. Research projects have been conducted on the AES problem under deterministic load and parameter deviations [2,3], while stochastic analyses have been largely applied to terrestrial power systems for reliability assessment [4,5] and for uncertainty analysis of load and system performance [6–11].

The most common approach for stochastic simulation in large-scale systems is Monte Carlo integration. The technique is simple to implement, using forward simulations of the system response. The so-called quasi-Monte Carlo techniques [16] regularize the random points, so as to achieve improved convergence. Alternatives we consider and compare in this paper are the Galerkin and Collocation projection techniques using polynomial chaos. The Galerkin approach yields an explicit functional relationship between random variables and stochastic solutions, represented in terms of a spectral decomposition. In the Collocation technique, the stochastic solutions can be obtained from simulations at nodal points in the random space.

The method of generalized Polynomial Chaos (gPC), based on the Galerkin projection [12–15], has been successfully applied for stochastic analysis in various applications, such as finite elements in solid mechanics [12], fluid dynamics [16], and electrical circuits [17]. Major advantages of the gPC technique are that a probability density function, as well as statistical moments of system variables, can be obtained explicitly after solving nodal system equations. The limitation associated with the gPC is the expansion complexity of non-polynomial terms onto the orthogonal polynomial-chaos basis.

* Corresponding author at: Division of Applied Mathematics, Brown University, 182 George Street, Box F, Providence, RI 02912, USA. Tel.: +1 401 863 1217; fax: +1 401 963 3369.
E-mail addresses: pradya@mit.edu (P. Prempraneerach), hover@mit.edu (F.S. Hover), mistetri@mit.edu (M.S. Triantafyllou), gk@dam.brown.edu (G.E. Karniadakis).

0951-8320/$ - see front matter © 2010 Elsevier Ltd. All rights reserved.
doi:10.1016/j.ress.2010.01.012

The Probabilistic Collocation Method (PCM), based on the Collocation projection approach of polynomial chaos, has been used for examining the transient behavior of utility power systems [6,7] and ocean circulation [18]. The theory underlying the PCM, here called the Full-grid PCM, is the numerical Gauss-quadrature, an efficient numerical integration technique [19] for low-dimensional problems. When the dimension of stochastic inputs increases as in a large-scale system, the computational cost of the Full-grid PCM becomes prohibitive. Therefore, another collocation technique of numerical integration-Smolyak quadrature [20,21] (referred to as the Sparse-grid PCM) has been in recent use.

The accuracy of stochastic solutions from both techniques deteriorates quickly, when there exists a low regularity, e.g., a discontinuity, in the stochastic solutions. To this end, the Multi-Element technique or the h-type refinement of the random space in both approaches gives a promising result to further improve solution accuracy [14,22].

In this paper, Section 2 introduces the concept of polynomial chaos from both Galerkin and Collocation approaches as well as their Multi-Element formulations. The performance of these techniques is compared on several test cases, and two multi-rate dynamical power systems in Section 3. Section 4 presents a brief summary and discussion of the main findings.

2. Polynomial chaos methods

According to the Cameron–Martin theorem [23], the so-called Wiener–Askey polynomial chaos expansion can approximate and describe all stochastic processes with finite second-order moment; this is satisfied for most physical systems. The Askey scheme of polynomials contains various classes of orthogonal polynomials, and their associated weighting functions are identical to the probability density function of different distributions. As shown in [15], these Askey polynomial schemes yield an optimal (exponential) convergence of stochastic solutions for their corresponding probability distributions. First, let us define a general form of the Stochastic Differential Equation (SDE) in a complete probability space $(\Omega, \mathcal{F}, P)$, where Ω is the event space, P the probability measure, and $\mathcal{F}$ the probability distribution associated with P, as follows:

$$\mathcal{L}(t,\omega;u) = f(t,\omega), \tag{1}$$

where t is defined within a temporal domain $[0,T]$, T is the final time, $\omega \in \Omega$ ranging within the support of $\mathcal{F}$, $\mathcal{L}$ is a linear or nonlinear operator including the differentiation, and f is a forcing term. Expressing the SDE in this form, uncertainties can be incorporated in both the L operator and f such that the stochastic solution, $u(t,\omega)$, reveals a propagation of these uncertainties in the system through time. Throughout this study, $\xi_i(\omega)$ for $i=1,\ldots,d$ are assumed to be d-dimensional independent, identically distributed (i.i.d.) continuous random variables.

In a realistic situation, uncertainty of system parameters and loads tend to vary within a specified range. Therefore, the uniform and exponential distributions are most suitable to represent these uncertainties rather than the Gaussian distribution, related to the Hermite chaos, as described in [17]. Our stochastic analysis of power systems is associated with the i.i.d. *uniform* distribution $\xi \in U[-1,1]$. Next, we describe the underlying theory of these stochastic algorithms as well as their advantages and disadvantages from an implementation perspective.

2.1. Galerkin projection

The main concept of the generalized Polynomial Chaos (gPC) is to employ the spectral expansion of $u(t,\omega)$ and $f(t,\omega)$ in terms of the weighted sum of orthogonal polynomial bases, associated with their modal coefficients. A general second-order random process can be concisely expressed in the following form:

$$u(t,\omega) = \sum_{i=0}^{\infty} u_i(t)\phi_i(\xi(\omega)), \tag{2}$$

where ϕ_i denotes the polynomial basis from the Wiener–Askey polynomial chaos, expressed as a function of a d-dimensional random variable ξ. This form of expansion converges optimally in the L_2 sense. The type of the proper polynomial basis to be employed depends on the pdf of the random variable ξ. This is dictated by a "correspondence principle" where the form of the orthogonality weight in the polynomials matches the corresponding probability measure [15]. For example, the classical case is the Hermite polynomials whose weight is the Gaussian distribution; similarly, the Legendre polynomials correspond to uniform distribution, the Laguerre polynomials to exponential distributions, the Jacobi polynomials to Beta distributions, etc. This correspondence can be extended to non-analytic polynomials beyond the Askey class of polynomials, as first proposed in [32].

The $\mathbf{u}_i(t)$ is the ith modal coefficient, the set from which statistics can be directly calculated. In numerical implementation, the expansion onto the orthogonal polynomial basis must be truncated at P terms; $P=(d+p)!/d!p!$, where d and p, respectively, are the dimension of random variable ξ and the highest order of the polynomial chaos. With the assumption of $\xi_i \in U[-1,1]$, the Legendre polynomial chaos is chosen as the basis, ϕ_i, because of its optimal convergence property. Then, we substitute this spectral expansion of u and f into Eq. (2) and project this equation onto the p-order polynomial chaos basis using the Galerkin projection, $\langle \mathcal{L}, \phi_i \rangle = \langle f, \phi_i \rangle$ for $i = 0,\ldots,P$. Due to the orthogonal property of the Wiener–Askey polynomial chaos we have

$$\langle \phi_{\mathbf{i}}, \phi_{\mathbf{j}} \rangle = \langle \phi_{\mathbf{i}}^{\mathbf{2}} \rangle \delta_{ij}, \tag{3}$$

where δ_{ij} is the Kronecker delta and $\langle \cdot,\cdot \rangle$ represents the inner product on the support of the random variable ξ. As a result, we obtain a set of $(P+1)$ coupled deterministic equations for the modal coefficients.

Once the time integration of the modes is complete, the first and second moments (i.e., the mean and variance solutions) can be directly calculated from the zero mode and from a summation of the squared modal amplitudes, each multipled by $\langle \phi_i^2 \rangle$, as shown below:

$$\mu_1(u(t,\xi)) = u_0(t), \tag{4}$$

$$\mu_2(u(t,\xi)) = \sum_{i=1}^{P} u_i^2(t) \langle \phi_i^2 \rangle. \tag{5}$$

The accuracy of the stochastic solution can be improved by increasing the polynomial order – "p-type" refinement – which leads to an exponential convergence rate for continuous solutions.

2.1.1. Multi-element gPC (MEgPC)

According to Wan and Karniadakis [14], if the domain of random inputs (ω) is decomposed into multiple elements, the accuracy of stochastic solutions can be further improved, especially in the cases of discontinuity in stochastic solutions or of long-time integration. As a result of this "*h-type*" refinement, the local integration error at each time step can be reduced and the solution can be approximated more accurately within smaller domains. We will briefly explain the basic concept of the Multi-Element gPC (MEgPC) [14] with d-dimensional random variables.

First, let $\boldsymbol{\xi}(\omega) = [\xi_1(\omega),\ldots,\xi_d(\omega)]$, denote a vector of the uniform random variables in d dimensions. Second, we decompose

the domain of the random variable into N non-intersecting intervals or elements,

$$E^k = [a_1^k, b_1^k) \times \cdots \times [a_d^k, b_d^k) \quad \text{for } i = 1, \ldots, d. \tag{6}$$

The domain of each element is contained within a hypercube, $[a_1^k, b_1^k) \times \cdots \times [a_d^k, b_d^k)$, where a_i and b_i denote a lower and upper bound of the ith element, respectively. Therefore, we must scale the local random variables associated with each element ($\boldsymbol{\zeta}^{\mathbf{k}} = [\zeta_1^k(\omega), \ldots, \zeta_d^k(\omega)]$) accordingly with its conditional probability density function, $p_{\zeta^k} = 1/(b_i^k - a_i^k)$, where $i = 1, \ldots, d$ and $k = 1, \ldots, N$. The mapping of random variables from global to local domain (i.e., the element) is governed by the following relationship:

$$\zeta_i^k = \frac{b_i^k - a_i^k}{2}\xi_i^k + \frac{b_i^k + a_i^k}{2}, \tag{7}$$

where the global random variable, ξ_i^k, is contained within the $[a_i^k, b_i^k)$ range. The local random variable, ζ_i^k, is also a uniform random variable; therefore, we can apply the gPC with the Legendre polynomial chaos basis to solve the SDE, $\mathcal{L}(t, \boldsymbol{\zeta}(\boldsymbol{\omega}); u) = f(t, \boldsymbol{\zeta}(\boldsymbol{\omega}))$, locally in each of the N elements. Using Bayes' Rule and the total probability theorem, the m-order global statistical moments ($\mu_m(u(\xi))$) can be calculated from the m-order local statistics ($\mu_m(u(\zeta))$) as shown below:

$$\mu_m(u(t, \xi)) = \sum_{k=1}^{N} p_{\zeta^k} \mu_m(u(t, \zeta)). \tag{8}$$

There are several issues that need to be addressed for an accurate and efficient implementation of the aforementioned ideas. We define the original layout of elements as a "coarse" level, which we will refine by creating more elements. To this end, for simplicity in the numerical implementation we choose to split the element by half along the direction we refine. In order to decide when to refine we adopt two possible criteria. The first one employs the local gPC expansion and investigates the rate of convergenced by looking at the decaying of the coefficients, e.g., the last coefficient. If the decay is slow (given a pre-determined threshold) we proceed with the splitting of the element. Alternatively, we can compute the local variance in that particular element and if that is too large compared with some reference value we then split the element. Both criteria are effective but the latter is more economical in the collocation version of polynomial chaos as it avoids expensive multi-dimensional projections that the former method would require.

In addition, we need to assign the initial condition after splitting the random dimension into multiple elements, which can be done by solving the a linear system [14]. Let us denote the expansion of state variables at the coarse level, $\hat{x}^k(\xi^k) = \sum_{i=0}^{P} \hat{x}_i^k \phi_k(\xi^k)$ for k=1,…, N, for N elements. If we split each element into two sub-elements at the refined level, the state-variable expansion can be expressed as $\tilde{x}^k(\zeta^k) = \sum_{i=0}^{P} \tilde{x}_i^k \phi_k(\zeta^k)$ for k=1,…,2N. To assign the initial condition for $\tilde{x}_i^k$, we must solve the following linear system:

$$\begin{pmatrix} \phi_{00} & \phi_{10} & \cdots & \phi_{P0} \\ \phi_{01} & \phi_{11} & \cdots & \phi_{P1} \\ \vdots & \vdots & \ddots & \vdots \\ \phi_{0P} & \phi_{1P} & \cdots & \phi_{PP} \end{pmatrix} \begin{pmatrix} \tilde{x}_0 \\ \tilde{x}_1 \\ \vdots \\ \tilde{x}_P \end{pmatrix} = \begin{pmatrix} \sum_{i=0}^{P} \widehat{x}_i \phi_i(\zeta^0) \\ \sum_{i=0}^{P} \widehat{x}_i \phi_i(\zeta^1) \\ \vdots \\ \sum_{i=0}^{P} \widehat{x}_i \phi_i(\zeta^P) \end{pmatrix}, \tag{9}$$

where $\phi_{ij} = \phi_i(\zeta^j)$.

2.2. Collocation projection

The Probabilistic Collocation Method (PCM) is an alternative approach to solve stochastic equations using the polynomial chaos. Instead of expanding the stochastic solution onto the polynomial chaos basis, the Collocation approach evaluates the SDE at the abscissas of the polynomial chaos, i.e., the roots $\xi_i(\omega)$ of the Legendre polynomials, as follows:

$$\mathcal{L}(t, \boldsymbol{\xi}_{\mathbf{i}}(\omega); u) = f(t, \xi_i(\omega)). \tag{10}$$

The stochastic solutions are then computed according to a numerical quadrature with the weight function associated with a specified probability distribution. Therefore, when the systems become larger and more complex, the simplicity of the PCM framework, which is only repetition runs of the deterministic solver, results in a faster algorithm than the gPC, particularly in high dimension problems. In this section, two collocation techniques, Full- and Sparse-grid collocation, are explained in detail along with a framework for the multi-element technique.

2.2.1. Full-grid PCM (FPCM)

For the uniform random process, the Full-grid PCM (FPCM) relies on the non-equidistant abscissas of the Legendre polynomials for specifying the collocation points and the Gauss–Legendre quadrature rule for computing statistics. Similar to the p-refinement, the more collocation points per random dimension, N_c, the better the accuracy of stochastic solutions becomes. However, the collocation points from the full-tensor product in the full-grid PCM is non-nested, as illustrated in Fig. 1. When points at one level of N_c are re-used at a higher level, we say the points are nested.

The one-dimensional Gauss-quadrature formula, which is a well-known numerical integration technique, yields the exact integral for any function in a polynomial form of order less than or equal to $2N_c - 1$. An approximation of the d-dimensional integration by the full-tensor product, $\otimes$, of the one-dimensional Gauss–Legendre quadrature [19] is shown below:

$$\mu(u(t, \xi)) = \int_{\Omega} u(t, \xi) W(\xi)\, d\xi = \sum_{i_1=1}^{N_{c1}} \cdots \sum_{i_d=1}^{N_{cd}} u(t, \xi_{i_1} \ldots \xi_{i_d}) \times (w_{i_1} \otimes \cdots \otimes w_{i_d}), \tag{11}$$

where ξ_{i_j} and w_{i_j} are, respectively, the one-dimensional collocation points and associated weights of the N_{cj}-order polynomial chaos in the j dimension over a probability domain, Ω, and $u(t, \boldsymbol{\xi}_{\mathbf{i_j}})$ denotes the deterministic solution evaluated at these collocation points. For a high-dimensional random process, the number of collocation points in the full-grid PCM grows exponentially as a function of N_c^d to maintain the same degree of exactness; another quadrature rule with sparse structure, introduced next, can further reduce the computational burden.

2.2.2. Sparse-grid PCM (SPCM)

With the nested property of Chebyshev polynomials of the first kind, the Smolyak quadrature and the Clenshaw–Curtis formula forms can be used in the Sparse-grid PCM (SPCM) to significantly reduce the computational cost and to maintain the accuracy of stochastic solutions, especially in a system with large random dimensions.

In one dimension, the non-equidistant extreme points of the Chebyshev polynomials can be written in an analytical form as a cosine function [20]:

$$\xi_{Li} = -\cos\frac{\pi(i-1)}{n_L^1 - 1} \tag{12}$$

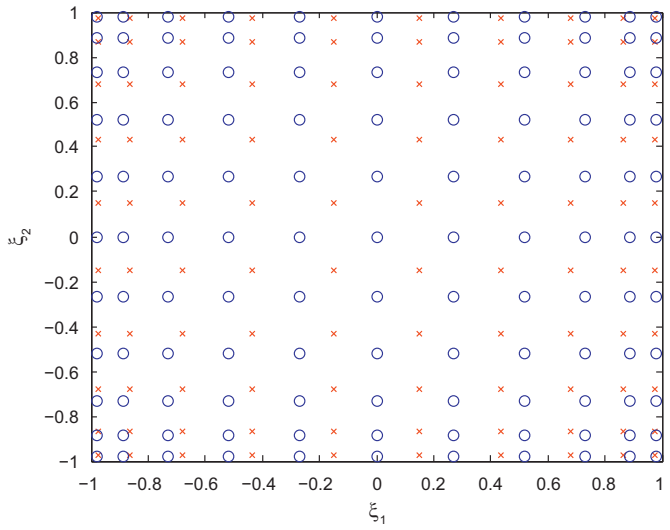

Fig. 1. Non-equidistant and non-nested abscissas of collocation points in the full-grid PCM with N_c=10 (cross) and N_c=11 (circle) in two random dimensions (ξ_1, ξ_2).

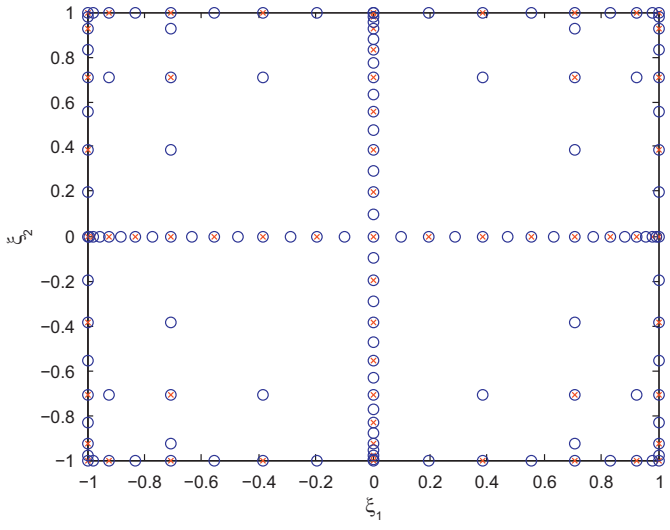

Fig. 2. Non-equidistant and nested collocation points for L=5 (cross) and L=6 (circle) of the sparse-grid PCM in the two random dimensions.

for $i=1,\ldots,L$, where n_L^1 denotes the number of L-level collocation points in one dimension. $n_L^1 = 2^{L-1}+1$, for $l \geq 2$. To approximate an integral, the sparse-grid PCM employs the weight, w_{Li}, from the Clenshaw–Curtis formulas as follows:

$$w_{Li} = \frac{2}{n_L^1 - 1}\left(1 + 2\sum\nolimits_{j=1}^{\prime(n_L^1-1)/2} \frac{1}{1-4j^2}\cos\frac{2\pi(i-1)j}{n_L^1-1}\right) \tag{13}$$

for $2 \leq i \leq n_L^1 - 1$ and $w_{L1} = w_{Ln_L^1} = 1/n_L^1(n_L^1-2)$. $\sum'$ notation denotes that the last term of the summation is divided by a factor of two. Instead of using the Gauss-quadrature, Smolyak's quadrature is used for calculating stochastic solutions.

Let us define a notation of the one-dimensional quadrature formula for the L level as follows: $Q_L^1 u = \sum_{i=1}^{n_L^1} u(\xi_{Li}) w_{Li}$. Then, the difference quadrature formula ($\Delta_L^1 u$) is defined as the difference of one-dimensional quadrature formula between the higher and lower level: $\Delta_k^1 u = (Q_k^1 - Q_{k-1}^1)u$. The d-dimension Smolyak quadrature formula [24] can be constructed as a function of either $\Delta_L^1 u$ or $Q_L^1 f$:

$$Q_L^d u = \sum_{|Li| \leq L+d+1} (\Delta_{L1}^1 \otimes \cdots \otimes \Delta_{Ld}^1)u$$

or (14)

$$Q_L^d u = \sum_{L \leq |Li| \leq L+d+1} (-1)^{L+d-|Li|-1} \binom{d-1}{|Li|-l} (Q_{L1}^1 \otimes \cdots \otimes Q_{Ld}^1)u.$$

From a numerical implementation point of view [24], expression (14) can be written explicitly in terms of nested grid points and weights as

$$Q_L^d u = \sum_{|Li| \leq L+d+1} \sum_{j_1=1}^{n_L^1} \cdots \sum_{j_d=1}^{n_L^d} w_{\mathbf{Lj}} u(\boldsymbol{\xi}_{\mathbf{Lj}}), \tag{15}$$

where $\boldsymbol{\xi}_{\mathbf{Lj}}$ denotes the d-dimensional vector of $(x_{L_1 j_1}, \ldots, x_{L_d j_d})$. Also, the nested weight can be written as

$$w_{\mathbf{Lj}} = \sum_{|L+k| \leq L+2d-1} z_{(L1+k1)j_1} \cdots z_{(Ld+kd)j_d}, \tag{16}$$

where $z_{(L+k)j_1} = w_{Lj}$ if k=1, or $z_{(L+k)j_1} = w_{(L+k-1)m} - w_{(L+k-2)n}$ if $k > 1$ and $\xi_{Lj} = \xi_{(L+k-1)m} = \xi_{(L+k-2)n}$.

The SPCM using the Clenshaw–Curtis formulas can provide an accurate result for integrating polynomial functions of orders up to $n_L^1 - 1$. Fig. 2 shows the characteristics of the nested collocation points of the SPCM in two random dimensions.

2.2.3. Multi-element PCM (MEPCM)

Parallel to the MEgPC, a basic concept of Multi-Element PCM (MEPCM [22]) is to divide the random variable into multiple elements such that the degree of randomness in the original space is reduced in proportion to the number of elements. Let us consider the orthogonal polynomial as a function of the random variable in a d-dimensional hypercube, $\boldsymbol{\xi} = [\xi_1, \ldots, \xi_d]$, where $\xi_i \in U[-1, 1]$ with a constant PDF of 1/2. By separating the random variable ($\boldsymbol{\xi}$) in the global level into N non-overlapping elements (E^k), the local element in a d-dimensional hypercube can be expressed as in Eq. (6). As a result, the local random variable (ζ^k) in each element can be computed by the mapping relationship, given in Eq. (7).

The main difference between the MEgPC and MEPCM is the method of mapping the initial condition from current-level meshes to those in a refined level. At each time step, the system solutions, $f(\xi_i)$, are evaluated only at the nodal points in the current-level meshes. If one of the elements in the current mesh is split into two new elements at the next time step, initial conditions of new elements can be either assigned directly from the original element in the case of $\boldsymbol{\xi}^k = \boldsymbol{\zeta}^k$ or, in the case of $\boldsymbol{\xi}^k \neq \boldsymbol{\zeta}^k$, we must solve the system at these new nodal points from an initial time. As a result, the original FPCM or SPCM, associated with the global random space, is decomposed into N sub-problems of the FPCM (ME-FPCM) or SPCM (ME-SPCM), corresponding to N local elements. We refer to Uniform ME-FPCM and ME-SPCM when the global random space is divided into N equally spaced elements.

Then, local statistical measures ($\mu_m(f(\zeta))$) in each element are computed by the Gauss quadrature formula for the FPCM and the Smolyak quadrature formula for the SPCM. To calculate the global mth moments ($\mu_m(f(\xi))$), Bayes' rule and the law of total probability can be applied as follows:

$$\mu_m(f(\xi)) = \int_{[1-1,1]^d} f^m(\xi) W(\xi)\, d\xi = \sum_{k=1}^{N} p_{\zeta^k} \int_{[-1,1]^d} f^m(\zeta^k) W(\zeta^k)\, d\zeta^k, \tag{17}$$

where the integral can be evaluated according to the Gauss–Legendre and the Smolyak quadratures for FPCM and SPCM, respectively.

3. Results

Generally, the accuracy of solution, the efficiency of computation, and the simplicity of implementation must be considered in comparing the performance of stochastic simulation algorithms. Foremost, a convergence study shows how accurate the stochastic solutions become as the governing parameters of these algorithms vary. The governing parameters of MC, gPC, FPCM, SPCM, and Multi-Element techniques are as follows: number of realizations (N_r), polynomial order (p), number of collocation points (N_c), level (L), and number of elements (N). Because the gPC and PCM methods both derive from quadrature rules, we expect that when $N_c \sim p$, similar errors are obtained for the two methods. The number of operations performed at each time step (or computational time to achieve a given accuracy) indicates the algorithm's efficiency. All numerical computations in this study are performed with the Microsoft C++ compiler on an Intel Pentium 4 3.0 GHz Processor. Note that the accuracy of stochastic solutions is limited in this paper by the numerical machine precision, which is on the order of 10^{-15}.

To study the rate of convergence, we use the L_2 norm difference between estimated and reference solutions of mean and variance, normalized by the L_2 norm of the reference solution. This normalized L_2 norm difference is similar to that defined in [15]. When the system is large and more complex, an analytical or exact stochastic reference solution is impossible to find. Then, the exact solution can be replaced by a computed solution for which the extrapolated error is at least an order of magnitude below that of the results presented. The error measurements of mean $\bar{y}$ and variance σ_y^2 solutions can be expressed as follows:

$$\varepsilon_{mean} = \frac{||\bar{y}(t) - \bar{y}_{exact}(t)||_2}{||\bar{y}_{exact}(t)||_2}, \tag{18}$$

$$\varepsilon_{var} = \frac{||\sigma_y^2(t) - \sigma_{y,exact}^2(t)||_2}{||\sigma_{y,exact}^2(t)||_2}. \tag{19}$$

3.1. Quadratic nonlinear first-order SDE

A first-order SDE is considered of the form

$$\frac{dy}{dt} = -ky^2 \quad \text{with } y(y-0) = y_0 = 1 \text{ and } t \in [0,5] \tag{20}$$

and a random variable decay rate $k = \bar{k} + \sigma_k \xi$, where ξ is a uniform distribution, $\xi \in U[-1,1]$. The deterministic solution is $y(t) = y_0/(y_0 kt + 1)$. Exact solutions of mean and variance, used as reference solutions, are

$$\bar{y}_{exact}(t) = \frac{1}{2t\sigma_k} \ell n \left| \frac{y_0 t(\bar{k} + \sigma_k) + 1}{y_0 t(\bar{k} - \sigma_k) + 1} \right|, \tag{21}$$

$$\sigma_{exact}^2(t) = \frac{y_0^2}{(1 + y_0 \bar{k} t)^2 + (y_0 \sigma_k t)^2} - \frac{1}{4t^2\sigma_k^2} \left(\ell n \left| \frac{y_0 t(\bar{k} + \sigma_k) + 1}{y_0 t(\bar{k} - \sigma_k) + 1} \right| \right)^2.$$

Consider the case where $\bar{k} = 2$, $\sigma_k = 2$, and $t \in [0,5]$. We examine the p-convergence of the gPC with $p = [1,2,3,4,5]$ and the FPCM with $N_c = [2,3,4,5,6]$, as shown in Fig. 3. The convergence rates are exponential in the order of $\mathcal{O}(e^{-p})$ for the gPC and of $\mathcal{O}(e^{-(N_c-1)})$ for the PCM. Both methods exhibit similar L_2 errors, and thus the relationship between gPC and PCM is $N_c = p+1$, as expected.

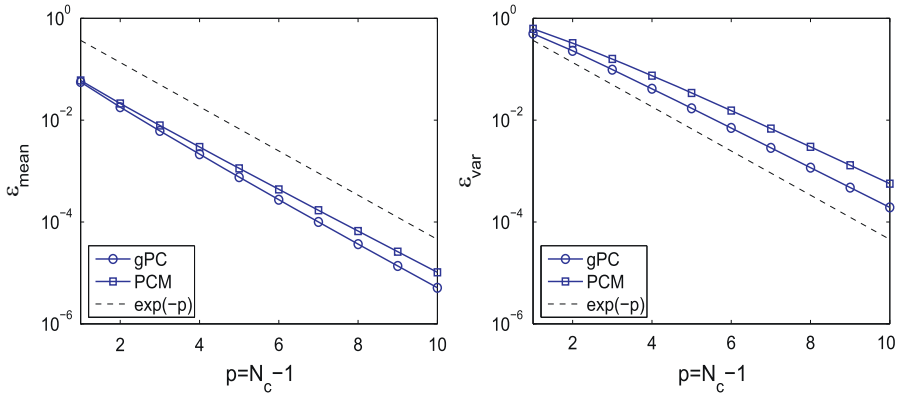

Fig. 3. Quadratic first-order SDE: plot of L_2 error of mean (left) and variance (right) as a function of polynomial order p for the gPC and N_c for the PCM.

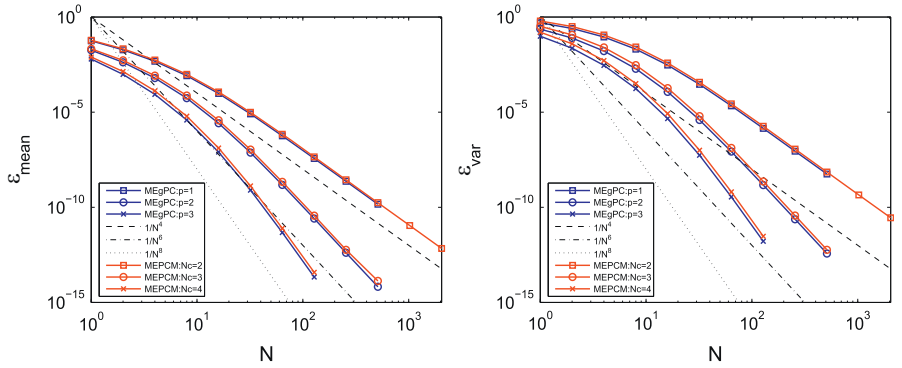

Fig. 4. Quadratic first-order SDE: plot of L_2 error of mean (left) and variance (right) errors as a function of number of elements, N, using MEPCM (thick line) and MEgPC (thin line).

For N-convergence using MEgPC with p=[1,2,3] and MEPCM with N_c=[2,3,4], the error convergence can be divided into two regimes: non-asymptotic and asymptotic. In the asymptotic, the convergence rates of MEgPC and MEPCM are approximated by $\mathcal{O}(N^{-2(p+1)})$ and $\mathcal{O}(N^{-2(N_c)})$, respectively, as shown in Fig. 4. Again, for the same accuracy, Fig. 4 confirms that $N_c=p+1$. For this simple problem, the gPC and PCM methods are nearly identical.

3.2. System of SDEs

Here we consider a system of three nonlinear SDEs, referred to as the Kraichnan–Orszag (K–O) system, first considered in [25] who employed the Wiener–Hermite expansion. It was reported that employing such an expansion leads to a divergence of the numerical solution from the true stochastic solutions as time increases. Recently, Wan and Karniadakis [14] have revisited this problem and resolved the divergence issue using a multi-element approach.

This system is represented by the ODEs:

$$\frac{dy_1}{dt} = y_1 y_3, \tag{22}$$

$$\frac{dy_2}{dt} = -y_2 y_3, \tag{23}$$

$$\frac{dy_3}{dt} = -y_1^2 + y_2^2. \tag{24}$$

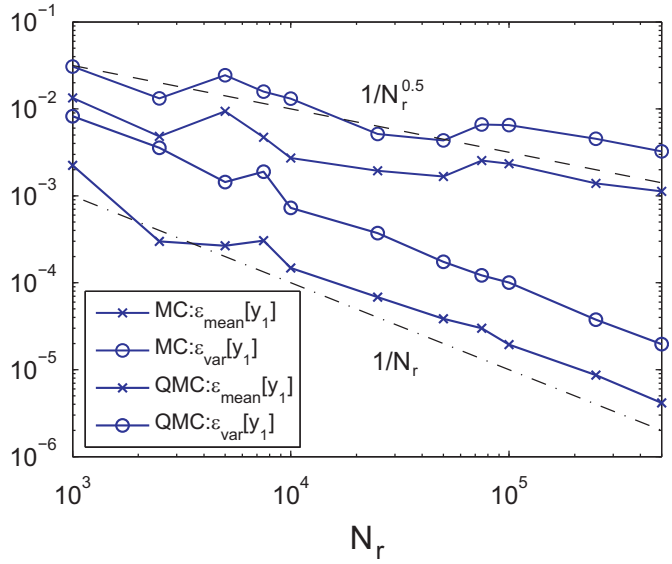

Fig. 5. Continuous K–O system: the L_2 norm error of mean and variance solutions as a function of N_r exhibits the algebraic convergence rate of $\mathcal{O}(N_r^{-1/2})$ using MC and of $\mathcal{O}(N_r^{-1})$ using QMC.

It is highly sensitive to the initial conditions; when the initial conditions are random variables, the stochastic solution can be either continuous or discontinuous in the initial conditions; see [14–22] for more details.

3.2.1. Continuous solutions in three random dimensions

We first investigate the convergence rate and efficiency of each algorithm in the case when the stochastic solutions are continuous. Let us assign the random initial conditions as follows: $[y_1(0,\xi),\ y_2(0,\xi),\ y_3(0,\xi)]=[[y_1(0,\xi),\ y_2(0,\xi),\ y_3(0,\xi)]=[\sqrt{2}/4+0.1\xi_1(\omega),\ \sqrt{2}/4+0.1\xi_2(\omega),\ \xi_3(\omega)]$. The reference solution is numerically computed from FPCM with N_c=80.

We consider the relationship of the convergence rate and computational cost as a function of the random dimension among five stochastic algorithms: (1) MC and QMC, (2) FPCM, (3) uniform ME-FPCM with N_c=[2,5,10], (4) SPCM, and (5) uniform ME-SPCM with L=5. As shown in Fig. 5, the MC and QMC convergence rates are $\mathcal{O}(N_r^{-1/2})$ and $\mathcal{O}(N_r^{-1})$, respectively, as expected.

Fig. 6 shows the exponential convergence of the FPCM and SPCM, described as functions of N_c and L, respectively; this exponential rate also holds as the random dimension increases. However, the convergence rate of SPCM can be classified into non-asymptotic and asymptotic regimes. Again, an empirical convergence relation for the asymptotic range is our main interest and asymptotic convergence of SPCM appears faster than convergence of FPCM. However, it should be noted that $N_c \approx 2^L$, so that a direct performance comparison must consider the computational cost versus the solution accuracy. Fig. 7 shows that the uniform ME-FPCM also has an asymptotic convergence regimes, with rate $\mathcal{O}((N/d)^{-2N_c})$. The error of the uniform ME-SPCM with L=5 as a function of N decreases faster than that of the ME-FPCM with N_c=5 because of more collocation points in the SPCM than in the FPCM for $L=N_c$ in three-dimensional random dimensions; this anomaly only happens for small number of dimensions. The convergence rate of the uniform MEgPC with p=1 again agrees well with that of the uniform ME-FPCM with N_c=2 due to the relationship between gPC and FPCM mentioned in the previous section.

Even though the convergence rate per dimension of the FPCM stays constant, its computation time grows with a cubic power of N_c in three random dimensions. For the uniform ME-FPCM with uniform distributed elements, the cost per fixed accuracy is always greater than that of the FPCM, as shown in Fig. 8. The computational cost of the SPCM increases even faster than that of the FPCM (N_c^d) and the uniform ME-SPCM may offer some benefit over the SPCM. The FPCM and MC provide the most and least efficient algorithms, respectively, in terms of the cost per accuracy, when the stochastic solutions are continuous and smooth.

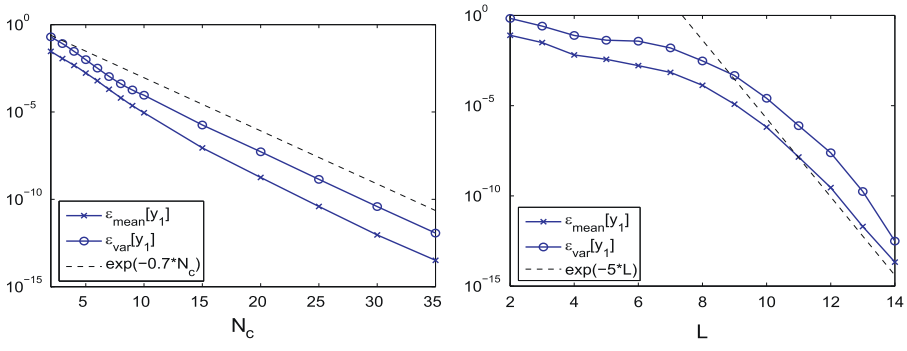

Fig. 6. Continuous K–O system: the L_2 norm error of mean and variance solutions with respect to collocation points using FPCM (left) and with respect to level using SPCM (right).

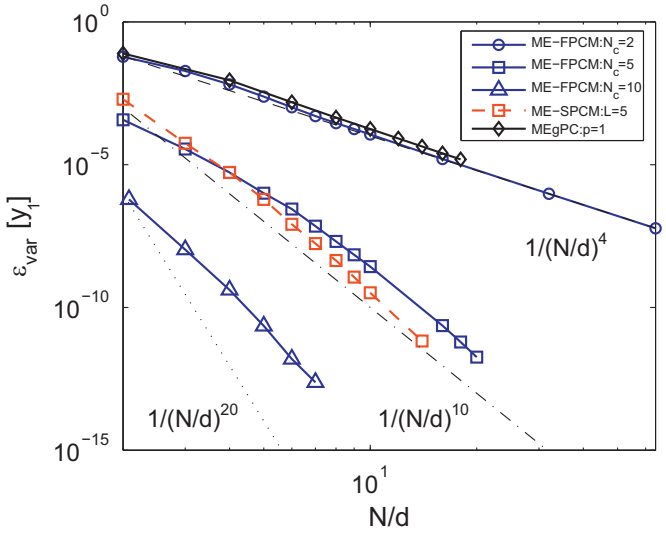

Fig. 7. Continuous K–O system: the L_2 error convergence of y_1 variance solutions as a function of number of elements per dimension, N/d, exhibits the algebraic convergence rate of $\mathcal{O}(N^{-4})$ for N_c=2, $\mathcal{O}(N^{-10})$ for N_c=5 and L=5, and $\mathcal{O}(N^{-20})$ for N_c=10, using the uniform ME-FPCM and ME-SPCM.

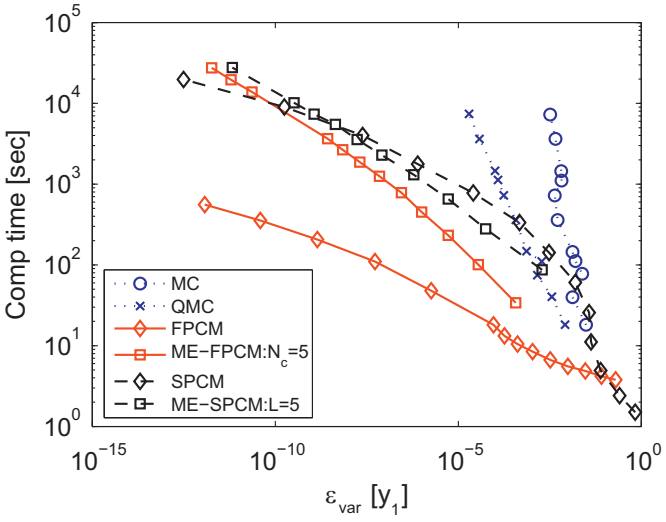

Fig. 8. Continuous K–O system at time (t=15): computational time versus error of variance, $\varepsilon_{var}[y_1]$, in MC, QMC, FPCM, ME-FPCM, SPCM, and ME-SPCM.

3.2.2. *Discontinuous solutions in three random dimensions*

With the three random initial conditions: $[\xi_1(\omega), 0.1\xi_2(\omega), \xi_3(\omega)]$ for the Kraichnan–Orszag system, discontinuity occurs on both the y_1 and y_2 planes [22]; thus the stochastic solutions are no longer smooth and continuous, and the time constants of mean and variance are longer than in the continuous case. The results from the QMC with $N_r = 5\times10^6$ for $t\in[0,15]$ are used as a reference solution to compute the convergence error.

We compare the performance among these five stochastic algorithms: (1) MC and QMC, (2) FPCM, (3) uniform ME-FPCM with N_c=[2,5,10], (4) SPCM, and (5) uniform ME-SPCM with L=5. Our main focus in this section is the effect of the sparseness of collocation points as well as of the uniform decomposition of random space. As illustrated in Fig. 9, MC and QMC again yield the convergence rate of $\mathcal{O}(N_r^{-1/2})$ and $\mathcal{O}(N_r^{-1})$, respectively. According to Fig. 10, an algebraic convergence rate of FPCM is on the order of $\mathcal{O}(N_c^{-1.2})$. Also, the SPCM yields an algebraic convergence, and its rate of convergence is on the order of $\mathcal{O}(L^{-9})$. The N-convergence

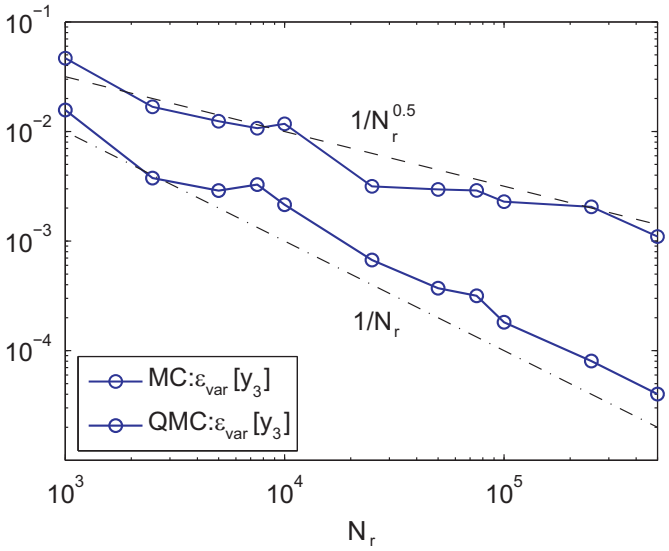

Fig. 9. Discontinuous K–O system: the L_2 error convergence of mean and variance solutions as a function of number of realizations, N_r, exhibits the algebraic convergence rate of $\mathcal{O}(N_r^{-1/2})$ using MC and of $\mathcal{O}(N_r^{-1})$ using QMC.

of the uniform ME-FPCM and ME-SPCM is shown in Fig. 11. The uniform ME-FPCM exhibits an algebraic convergence as a function of N/d, on the order of $\mathcal{O}((N/d)^{-1})$. In this case, the uniform ME-SPCM provides an algebraic convergence more prominently than the uniform ME-FPCM. One explanation of this better slope is that the sparse collocation points as a function of either level or element number are located much more at the boundary and the zero-axis of the hypercube, where the planes of discontinuity occur, than the full collocation points.

In terms of the cost for fixed accuracy, Fig. 12 shows that QMC is the most efficient, but the uniform ME-SPCM becomes more competitive against QMC in the higher accuracy region. The multi-element technique significantly improves the efficiency of both FPCM and SPCM in the presence of the discontinuities in stochastic solutions.

3.3. *An open-loop induction machine with the infinite bus*

The parametric uncertainty in a 200-hp induction machine directly connected to an infinite bus is considered in this section in terms of both error convergence and uncertainty propagation. The configuration of this system is shown in Fig. 13. This induction machine is a scaled-down version of the machine used in a propulsion system of the AES system, a model of which is considered in the next section. All parameters are given in Appendix I and [26]. The machine equations with quadratic nonlinearities consist of seven state variables: three rotor flux linkages per second $[\psi'^e_{qr}, \psi'^e_{dr}, \psi'^e_{0r}]$, the rotor's angular velocity $[\omega_r]$, and three stator or tie-line currents $[i^e_{qt}, i^e_{dt}, i^e_{0t}]$. Two states, ψ'^e_{0r} and i^e_{0t}, are uncoupled from the others.

In this study, the uncertainty of a rotor resistance (r'_r) is modeled as a time-dependent variable, i.e., a random process. Normally, the rotor resistance fluctuates with the operating temperature. Thus, we can represent this time-dependent parameter (r'_r) with the Karhunen–Loeve (KL) expansion [27], described in the following form: $r'_r(t,\omega) = \bar{r}'_r + \sigma_r \sum_{i=1}^{K} \sqrt{\lambda_i}\psi_i(t)\xi_i(\omega)$, where $\bar{r}'_r$ and σ_r are, respectively, the mean and standard deviation of the rotor resistance. The λ_i and ψ_i are an eigenvalue and an eigenfunction associated with the ith term of the KL expansion, truncated at K terms; $\xi(\omega)$ is the random

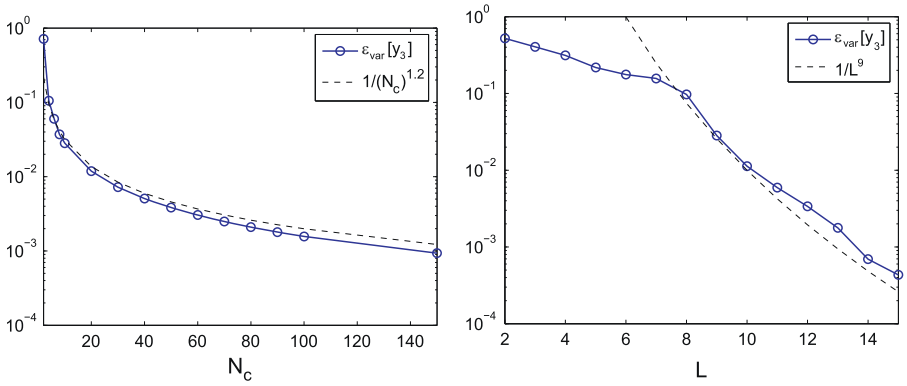

Fig. 10. Discontinuous K–O system: the L_2 norm error of mean and variance solutions with respect to collocation points using FPCM (left) and to level using SPCM (right).

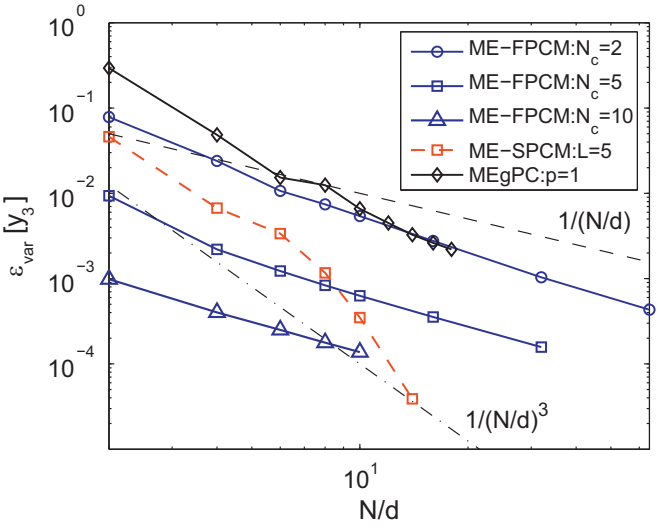

Fig. 11. Discontinuous K–O system: the L_2 error convergence of y_3 variance solutions as a function of N/d exhibits the algebraic convergence rate of $\mathcal{O}((N/d)^{-1})$ for N_c=[2,5,10] using uniform ME-FPCM and of at least $\mathcal{O}((N/d)^{-3})$ using uniform ME-SPCM.

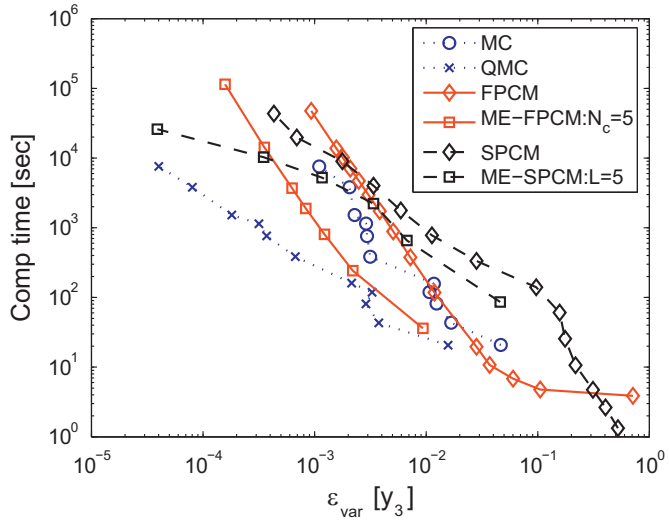

Fig. 12. Discontinuous K–O system at time (t=15): computational time versus error in variance for MC, QMC, FPCM, SPCM, uniform ME-FPCM, and uniform ME-SPCM.

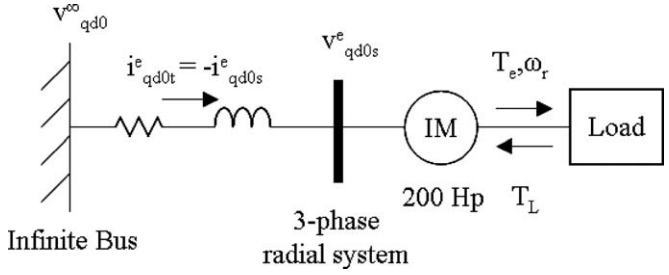

Fig. 13. A one-line diagram of the induction machine connected to the infinite bus through an RL tie line.

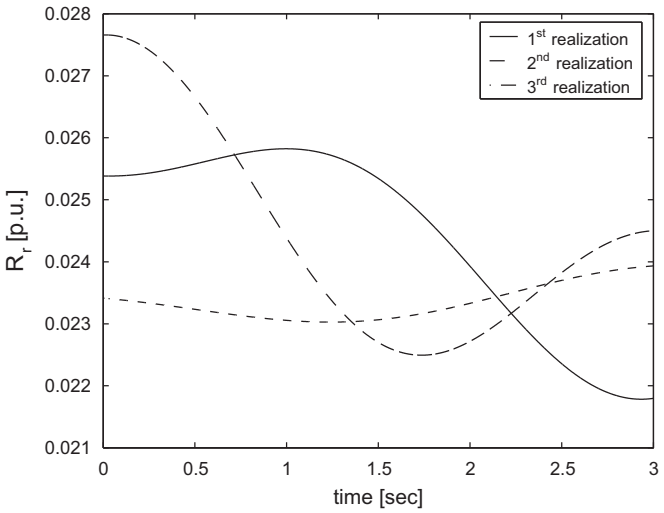

Fig. 14. Three realizations of the rotor resistance modeled by the three-term KL expansion using the exponential covariance function with L_c=10 s.

variable as a function of random seed ω. In this process, we assume that ψ_i and λ_i are determined from an exponential covariance function: $C(t_1,t_2)=\sigma_r^2 e^{-|t_2-t_1|/L_c}$, governed by the correlation length (L_c). In both cases, the values of $\bar{r}'_r$ and σ_r are 0.0261 p.u. and 0.01. Three realizations from the three-term KL expansion of r'_r are shown in Fig. 14. The random dimension, d, equals to three in this case.

The stochastic responses of the q-axis stator current, i^e_{qs}, during start-up dynamics of the 200-hp induction machine are shown in Fig. 15 for $t \in [0,3]$ s when the rotor resistance is a random process. These responses include fast transient dynamics from

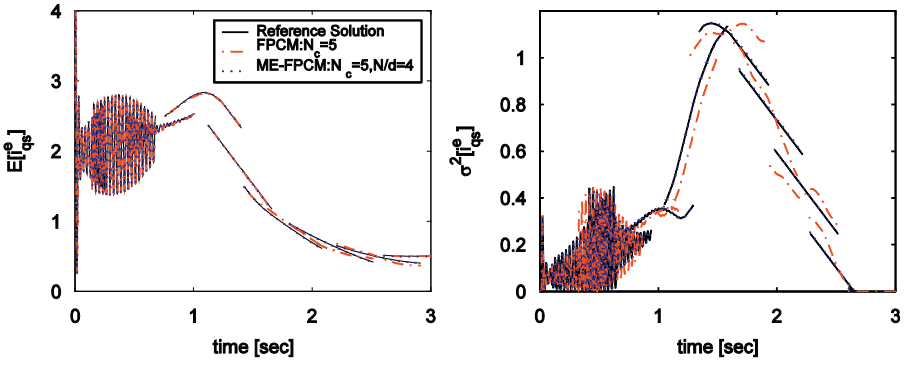

Fig. 15. Stochastic mean (left) and variance (right) of i^e_{qs} in per unit for the 200-hp induction machine.

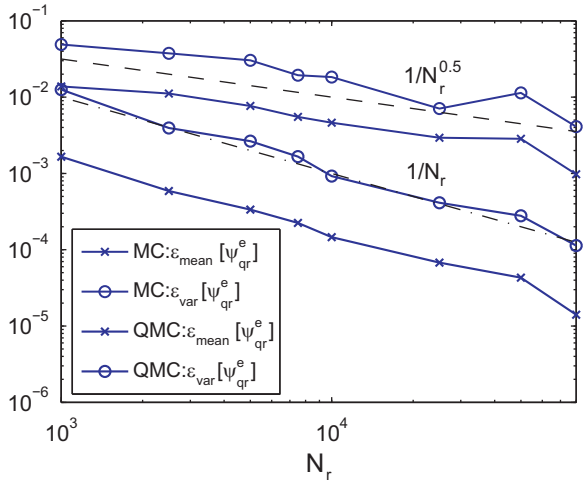

Fig. 16. Induction machine with infinite bus: the L_2 error in mean and variance as a function of the number of realizations, (N_r), exhibits the algebraic convergence rate of $\mathcal{O}(N_r^{-1/2})$ using MC and of $\mathcal{O}(N_r^{-1})$ using QMC.

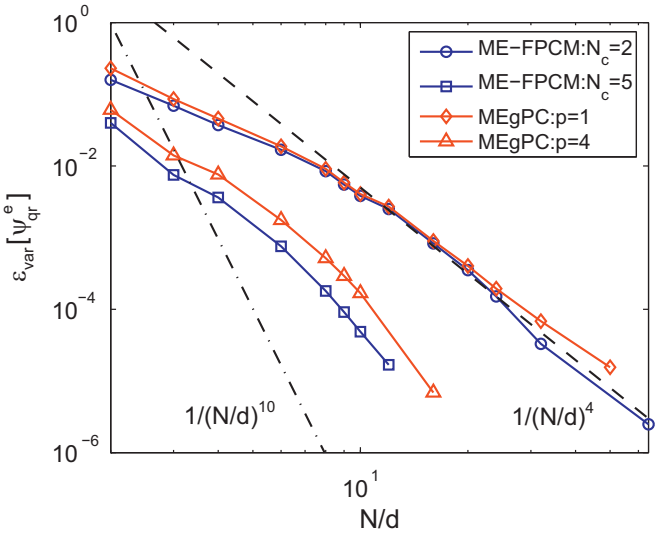

Fig. 17. Induction machine with infinite bus: the L_2 norm errors of variance as a function of the number of elements per dimension, N/d, using the uniform ME-FPCM and MEgPC, exhibit the algebraic convergence rate of $\mathcal{O}(N^{-4})$ for N_c=2 or p=1 and $\mathcal{O}(N^{-10})$ for N_c=5 or p=4.

electrical components, stator and rotor windings, and slow dynamics of a mechanical subsystem with rotor inertia. The solutions using the FPCM with N_c=5 diverge somewhat from the reference solution after 2 s, but the uniform ME-FPCM with N_c=5 and N/d=4 closely follows the reference solution. The reference solution in this case is obtained from the uniform ME-FPCM, with N_c=5 and N/d=32.

For a three-dimensional random process (with d=K=3) with $t \in [0,3]$ s, the convergence rate and computational efficiency are compared among these stochastic algorithms: (1) MC and QMC, (2) uniform ME-FPCM, and (3) uniform MEgPC. We did not perform sparse-grid calculations for this case. According to Fig. 16, the MC and QMC still yield the algebraic convergence rates of $\mathcal{O}(N_r^{-1/2})$ and $\mathcal{O}(N_r^{-1})$, respectively.

Again, the multi-element technique of gPC and FPCM with uniformly distributed elements exhibits both asymptotic and non-asymptotic convergence ranges, as shown in Fig. 17. For this non-stationary random input, the convergence rate in the asymptotic range of the uniform MEgPC and ME-FPCM are, respectively, on the order of $\mathcal{O}((N/d)^{-2(p+1)})$ and $\mathcal{O}((N/d)^{-2N_c})$, similar to the case with continuous solutions subjected to the stationary random input. In addition, the relationship N_c=p+1 between gPC and FPCM remains unchanged when the input is a random process. The FPCM still yields an exponential convergence rate on the order of $\mathcal{O}(e^{-0.3N_c})$, as shown in Fig. 18.

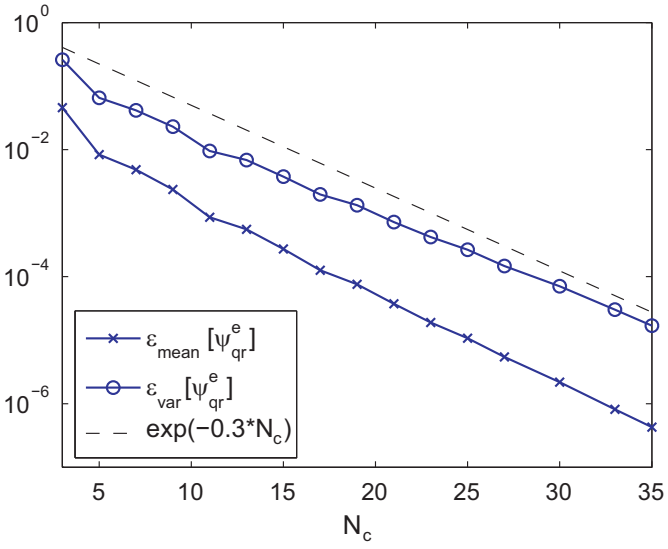

Fig. 18. Induction machine with infinite bus: the L_2 norm error of mean and variance solutions with respect to collocation points using FPCM.

The computational costs of FPCM and gPC increase in proportion to N_c^d nodal points and $(p+d)!/p!d!$ modes, respectively. Thus, gPC is more expensive than FPCM for the same accuracy due to the mode coupling that results from the Galerkin projection of polynomial chaos. Hence, the computational cost of the uniform MEgPC with $p=[1,4]$ is larger than that of the uniform MEPCM with $N_c=[2,5]$, as illustrated in Fig. 19.

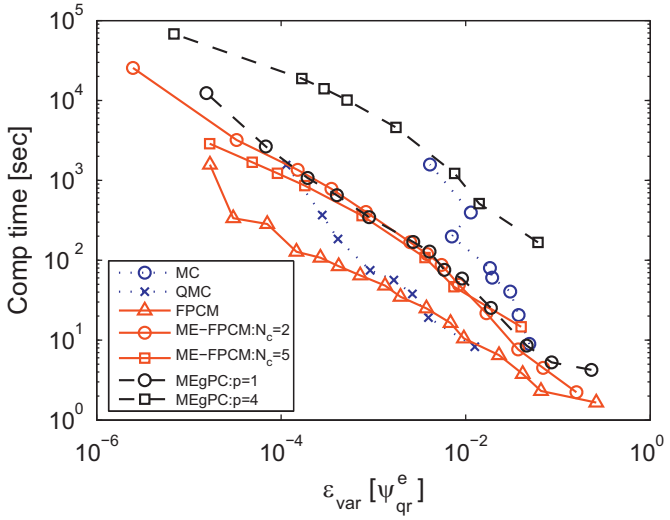

Fig. 19. Induction machine with infinite bus: computational time versus ε_{var} using MC, QMC, FPCM, uniform ME-FPCM with $N_c=[2,5]$, and uniform MEgPC with $p=[1,4]$.

3.4. AC power generation and propulsion systems

When the system becomes more complex, as in a shipboard power system, the order of the mathematical model can increase tremendously. We investigate now the performance of the best stochastic algorithms from Monte Carlo and Collocation approaches with a large-scale system. In this section, the configuration of the shipboard power system consists of an AC generation unit, a main three-phase radial bus, and two induction motors as the propulsion system. This configuration in Fig. 20 represents a scaled-down version of the power distribution system of a DDG-51 Navy destroyer [26]. The system consists of (1) a 3.125 MW Synchronous Machine (SM) driven by a simplified version of the Allison 501 gas turbine/governor, (2) the IEEE Type 2 exciter/voltage regulator for controlling the generator's voltage, (3) an RL tie-line, and (4) 200-hp and 150-hp Induction Machines (IM). Containing nonlinearities in both polynomial and trigonometric forms, this model is composed of 26 ODEs.

In this case, we assume six parameters in the system to be independent random variables, which includes $[r'_{kq}, r'_{fd}, r'_{kd}]$ of the synchronous machine, r'_r of both induction machines, and r_t of the tie line. All of these random variables, associated with the uniform distribution, are assumed to vary within $\pm 10\%$ of their nominal values. For this simulation, the generator is assumed to be initially in its steady-state condition and then suddenly the

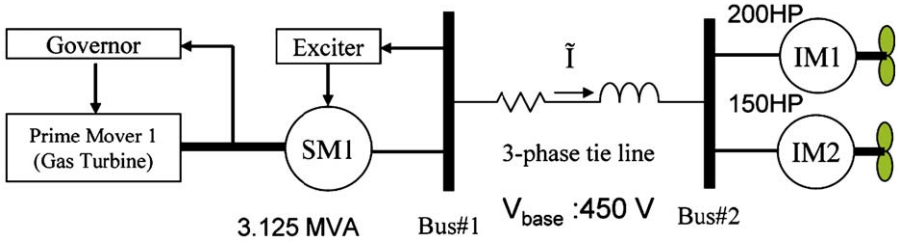

Fig. 20. A one-line diagram of the first configuration of the AC power distribution with two open-loop induction machines for studying the stochastic analysis with 6 dimensional random variables.

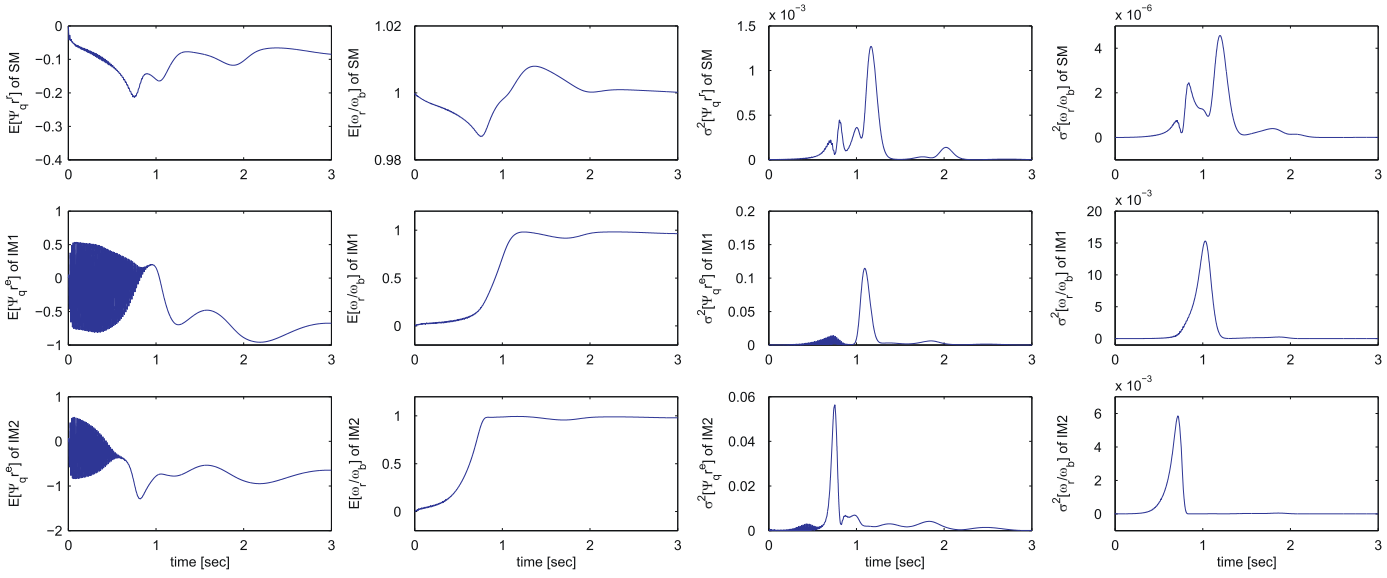

Fig. 21. The reference stochastic mean (left three columns) and variance (right three columns) solutions of the q-axis stator flux linkage and normalized rotor speed of SM, IM1, and IM2 in per unit, obtained from QMC with $N_r=1.2\times10^6$.

two induction machines start from rest at 0 s. The start-up transient of the two motors, similar to the previous section, as well as an interaction among electric machines can be seen in Fig. 21 for $t \in [0,3]$ s. At first, the speed of the synchronous machine drops and then the exciter compensates for an error in the bus voltage by speeding up the generator before bringing the synchronous machine's speed back to its steady-state operation of one per unit. In the first second, the start-up transient of both induction machines dies out. Subsequently, the interactions between synchronous and induction machines are illustrated in the responses of the q-axis stator flux linkage of all machines. The variance of all states of both motors contains a high peak directly before reaching the steady state. This characteristic implies that the open-loop response, especially immediately after the start-up transient, is sensitive to the parameter variation. With the closed-loop control of the exciter, the responses of the synchronous machine's variance have a smaller peak magnitude compared with those of the induction machines.

To study the numerical performance of stochastic algorithms—QMC, FPCM, SPCM, and uniform ME-SPCM—with this large-scale system, the convergence rate and computational efficiency are again considered. In this case, the reference solution is obtained from the QMC with $N_r = 3 \times 10^6$. The error plots of the SM q-axis stator flux linkage per second (Ψ^r_{qr}) using the QMC are shown in Fig. 22. In this system, the algebraic convergence rate of $\mathcal{O}(N_r^{-1})$ is again obtained from the QMC. For the FPCM and SPCM methods, Fig. 23 illustrates the L_2 errors of (Ψ^r_{qr}). The rate of convergence per random dimension using FPCM and SPCM is exponential with $\mathcal{O}(e^{-(1.8\times N_c)})$ or $\mathcal{O}(e^{-(1.8\times L)})$. From an efficiency aspect, the computing time per variance accuracy of all algorithms, illustrated in Fig. 24, can be used for the performance comparison among these stochastic algorithms. For this large-scale system, the computational cost of the SPCM is an order of magnitude less than that of the FPCM for the same accuracy. Furthermore, the SPCM also becomes more efficient than the QMC in the high-accuracy region. Unlike the results with the small model in Section 3.2.1, the uniform ME-SPCM improves the solutions' accuracy but at a higher computational cost than the SPCM.

4. Summary and discussion

We have presented several algorithms for solving stochastic ODEs, with applications to electromechanical power systems. For simplicity in the implementation we have modeled uncertainties by uniform random variables, which we assumed to be independent. Given the last assumption, we can readily replace the uniform random variables to other types following a Beta distribution, an exponential distribution, etc., by employing the proper polynomial basis from the Askey class of polynomials [15]. The extension to arbitray pdf using numerical procedures to

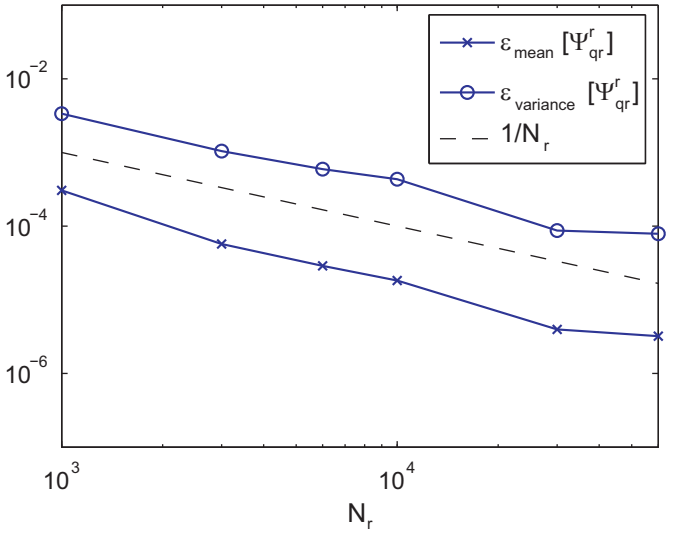

Fig. 22. AC power generation and propulsion systems: for six random dimensions, the L_2 error in x_1 or ψ^r_{qr} is $\mathcal{O}(N_r^{-1})$ using QMC.

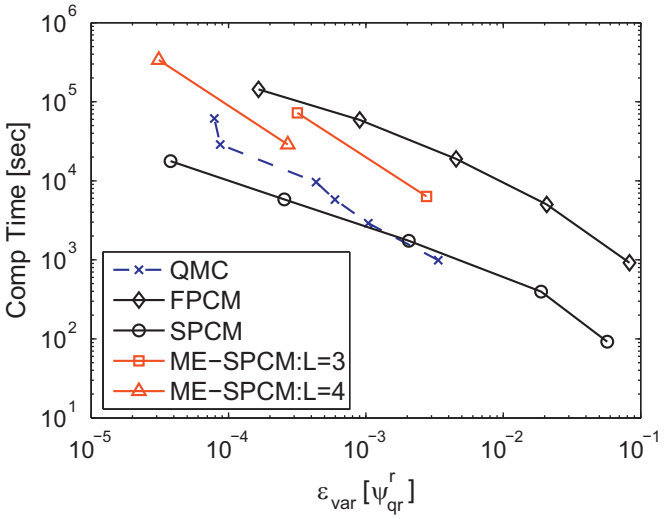

Fig. 24. AC power generation and propulsion systems: for six-dimensional stationary random inputs, the computational time per variance accuracy of the QMC, FPCM, SPCM, and uniform ME-SPCM methods.

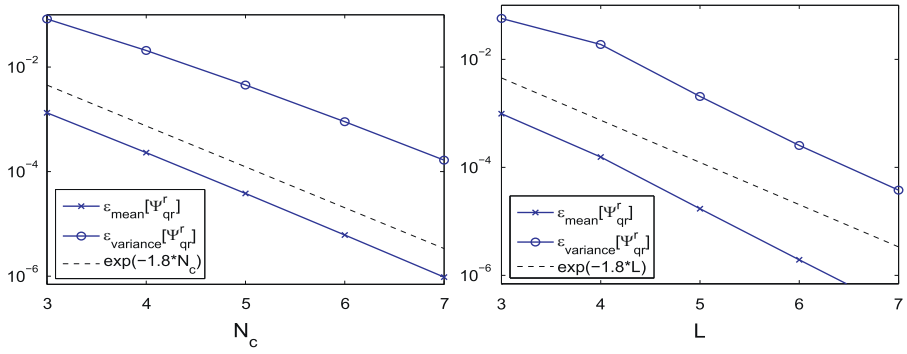

Fig. 23. AC power generation and propulsion systems: for six-dimensional random dimensions, the L_2 errors in x_1 or ψ^r_{qr} are on the order of $\mathcal{O}(e^{-1.8N_c})$ using FPCM (left) and of $\mathcal{O}(e^{-1.8L})$ using SPCM (right).

Table 1
Summary of the best stochastic algorithm for various systems in Section 3.

Section	Best stochastic algorithms	Comment
3.2.1	(1) FPCM	Smooth function and low dimension — good for quadratures
3.2.2	(1) QMC, (2) ME-SPCM	Known discontinuities and multi-element may align with discontinuities
3.3	(1) FPCM, (2) ME-FPCM	Smooth function and low dimension
3.4	(1) SPCM, (2) QMC	Smooth function and dimension is high enough that N_c^d of FPCM is large

compute orthogonal polynomials on-the-fly is also possible using the techniques presented in [32]. However, the extension to dependent random variables is non-trivial and very little work on this subject has been done so far, e.g., see [33] and references therein. Similarly, no work has been done yet on employing mixed random variables following different pdfs.

Assuming sufficient regularity in the stochastic solutions, both Galerkin and Collocation approaches of polynomial chaos provide exponential convergence in the errors of the mean and the variance; which algorithm performs the best depends on the problem considered. This fast convergence translates into savings of orders of magnitude compared with traditional Monte Carlo methods, for a small number of random dimensions. The use of sparse grids in the Collocation approach leads to enhanced efficiency enabling simulation in higher dimensions, but for a large number of random inputs the Monte Carlo method remains the most efficient approach. Table 1 summarizes the best stochastic algorithm for different systems in Section 3.

Table 2 summarizes the convergence rates of these algorithms for both continuous and discontinuous stochastic solutions. The convergence rates of all algorithms are described as functions of their governing parameters and an arbitrary constant (c), depending on the solution smoothness. The p and N_c or L parameters of the Galerkin and Collocation techniques are given per random dimension, where as the total number N of elements of the multi-element technique is normalized by the random dimension. Interestingly, the multi-element techniques have convergence for the discontinuous K–O system that do not depend on the polynomial order.

In fact, in the presence of discontinuities, both the Galerkin and Collocation approaches lose their exponential convergence. In this case, the decomposition of the random space into N d-dimensional elements provides an effective treatment, especially if it is combined with *adaptive domain decomposition*. In the present paper, we used uniform partitioning of elements, and realized some improvements in the solution accuracy. In adaptive domain decomposition, elements that exhibit large local variance are split into sub-elements according to a pre-specified criterion, e.g., targeting uniform values of variance everywhere; see [14,22]. This adaptive multi-element procedure is also very effective for *long-time integration* as polynomial chaos converges non-uniformly in time and hence higher resolution is required to maintain fixed accuracy for *all* times. This situation is similar to the numerical discretization of time-dependent partial differential equations, e.g., in the advection equation, where phase errors grow in time unless higher resolution is adaptively provided [28]. We have implemented such adaptive multi-element polynomial chaos procedures for the systems we have considered in the current paper and preliminary results suggest that the most effective approach is the multi-element probabilistic collocation approach (MEPCM); this is also consistent with the findings of Foo et al. [22]. The precise adaptivity criterion is crucial for a robust stategy and we are currently working towards this goal; it seems, however, that using the local variance computed element-wise as sensitivity index is the most economical approach to adaptive partitioning.

Table 2
Summary of the convergence rates for various stochastic algorithms in the case of continuous and discontinuous stochastic solutions, where c is a constant, related to the regularity of the solution.

Stochastic algorithms	Convergence rate for continuous	Convergence rate for discontinuous
MC	$\mathcal{O}(N_r^{-1/2})$	$\mathcal{O}(N_r^{-1/2})$
QMC	$\mathcal{O}(N_r^{-1})$	$\mathcal{O}(N_r^{-1})$
gPC	$\mathcal{O}(e^{-p})$	$\mathcal{O}(p^{-c})$
FPCM	$\mathcal{O}(e^{-(N_c-1)})$	$\mathcal{O}((N_c-1)^{-c})$
SPCM	$\mathcal{O}(e^{-L})$	$\mathcal{O}(L^{-c})$
MEgPC	$\mathcal{O}((N/d)^{-2(p+1)})$	$\mathcal{O}((N/d)^{-c})$
ME-PCM	$\mathcal{O}((N/d)^{-2N_c})$	$\mathcal{O}((N/d)^{-c})$

Finally, we comment on the "curse-of-dimensionality". Polynomial chaos methods are very effective in low dimensions but in high dimensions their fast convergence degrades very rapidly. The use of sparse grids alleviates the situation but only slightly, so for more than 10 or 20 dimensions the Monte Carlo method may be more efficient for the same accuracy. Recent work in [34,35] has addressed this issue where polynomial chaos methods are combined with ANOVA (ANalysis Of VAriance) to truncate the expansion at some "effective" dimension. Preliminary results show that the good efficiency of polymial chaos methods can be extended up to 500 dimensions at least for some classes of problems. Future work on modeling electromechanical power systems should address this important issue.

Acknowledgment

This work was supported by the Office of Naval Research (N00014-02-1-0623 ESRDC Consortium).

Appendix A

For the propulsion system, we briefly describe the formulation of a general mathematical model for the symmetrical three-phase squirrel-cage induction machines with four poles and three-phase windings in both the stator and rotor connected in a wye configuration [29,26]. The governing equations are written in the $qd0$ synchronous reference frame (denoted by superscript e). The voltage equations of the stator and rotor windings can be written as

$$\mathbf{v}^e_{qd0s} = -\mathbf{r}_s\mathbf{i}^e_{qd0s} + \frac{\omega_e}{\omega_b}\mathbf{T}_1\psi^e_{qd0s} + \frac{p}{\omega_b}\psi^e_{qd0s}, \tag{25}$$

$$\mathbf{v}'^e_{qd0r} = \mathbf{r}'_r\mathbf{i}'^e_{qd0r} + \frac{\omega_e-\omega_r}{\omega_b}\mathbf{T}_1\psi'^e_{qd0r} + \frac{p}{\omega_b}\psi'^e_{qd0r}, \tag{26}$$

where $\mathbf{v}^e_{qd0s}$, $\mathbf{i}^e_{qd0s}$, $\psi_{qd0s}{}^e$, and $\mathbf{v}'^e_{qd0r}$, $\mathbf{i}'^e_{qd0r}$, ψ'^e_{qd0r} are the stator and rotor variables of voltage, current, and flux, expressed in a vector form as $\mathbf{f}^e_{qd0s}=[f^e_{qs},f^e_{ds},f^e_{0s}]^T$ and $\mathbf{f}'^e_{qd0r}=[f'^e_{qr},f'^e_{dr},f'^e_{0r}]^T$, respectively. The resistance matrices $\mathbf{r}_s$ and $\mathbf{r}'_r$ are $diag[r_s, r_s, r_s]$ and $diag[r'_r, r'_r, r'_r]$. ω_r and ω_b are the rotor angular and base velocities; the synchronous speed ω_e is the same as ω_b in the absence of a controller. The positive direction of stator current is assumed to be outward from the stator winding. The prime symbol denotes that the rotor variables are scaled by a stator to rotor turn ratio.

The equations of flux linkage per second are

$$\psi^e_{qd0s}=-\mathbf{X}_{ls}\mathbf{i}^e_{qd0s}+\psi^e_{mqd}, \tag{27}$$

$$\psi^e_{qd0r}=\mathbf{X}'_{lr}\mathbf{i}'^e_{qd0r}+\psi^e_{mqd}, \tag{28}$$

where the flux leakage matrices $\mathbf{X}_{ls}$ and $\mathbf{X}'_{lr}$ are $diag[x_{ls},x_{ls},x_{ls}]$ and $diag[x'_{lr},x'_{lr},x'_{lr}]$. We write $\psi^e_{mqd}=-\mathbf{X}_b\mathbf{i}^e_{qd0s}+\mathbf{A}_r\psi^e_{qd0r}$, where $\mathbf{X}_b=diag[x_b,x_b,0]$ with $x_b=(x_m x'_{lr})/(x_m+x'_{lr})$, and $\mathbf{A}_r=diag[x_b/x'_{lr}, x_b/x'_{lr}, 0]$. x_m is the mutual inductance of the stator and rotor.

The dynamics of the mechanical subsystem can be written as

$$p\omega_r=\frac{\omega_b}{2H}(T_e-T_L), \tag{29}$$

where $T_e=\psi^e_{qs}i^e_{ds}-\psi^e_{ds}i^e_{qs}$ and T_L are the electromagnetic and load torques, respectively. The p denotes a differential operator. The rotor inertia (in seconds) is H.

The mathematical model of a three-phase salient-pole synchronous machine, consisting of linear magnetic circuits and neglecting any saturation [29,26], are described below; this system is used as the power generation in the power system. The fields produced by the winding currents are assumed to be sinusoidally distributed around the airgap, ignoring the space harmonics. The rotor windings consist of the field winding (fd) and damper windings (kq and kd), and the stator windings (qs,ds,0s) are symmetrical. The voltage equations of the stator and rotor windings expressed in the $qd0$ rotor reference frame can be written as the following:

$$\mathbf{v}^r_{qd0s}=-\mathbf{r}_s\mathbf{i}^r_{qd0s}+\frac{\omega_r}{\omega_b}\mathbf{T}_1\psi^r_{qd0s}+\frac{p}{\omega_b}\psi^r_{qd0s}, \tag{30}$$

$$\mathbf{v}'_{qdr}r=\mathbf{r}'_r\mathbf{i}'^r_{qdr}+\frac{p}{\omega_b}\psi'^r_{qdr}, \tag{31}$$

where ($\mathbf{v}^r_{qd0s}$, $\mathbf{i}^r_{qd0s}$, ψ^r_{qd0s}) and ($\mathbf{v}'^r_{qdr}$, $\mathbf{i}'^r_{qdr}$, ψ^r_{qdr}) are the stator and rotor variables of voltage, current, and flux, expressed in a vector form as $\mathbf{f}^r_{qd0s}=[f^r_{qs},f^r_{ds},f^r_{0s}]^T$ and $\mathbf{f}'^r_{qdr}=[f'^r_{kq},f'^{fd}_{dr},f'^r_{kd}]^T$, respectively. The resistance matrices $\mathbf{r}_s$ and $\mathbf{r}'_r$ are $diag[r_s,r_s,r_s]$ and $diag[r'_{kq}, r'_{fd}, r'_{kd}]$. Again, the $\mathbf{T}_1$ matrix is used with voltage terms, induced by the speed due to a reference frame transformation. The negative sign in the stator voltage and flux linkage equations represent an assumption that the positive direction of stator current is outward from the stator winding.

The equations of flux linkage per second are given below:

$$\psi^r_{qd0s}=-\mathbf{X}_{ls}\mathbf{i}^r_{qd0s}+\psi^r_{mqd}, \tag{32}$$

$$\psi^r_{qd0r}=\mathbf{X}'_{lr}\mathbf{i}'_{qd0r}r+\mathbf{T}_2\psi^r_{mqd}, \tag{33}$$

where the flux leakage matrices $\mathbf{X}_{ls}$ and $\mathbf{X}'_{lr}$ consequently are $diag[x_{ls},x_{ls},x_{ls}]$ and $diag[x'_{lkq}, x'_{lfd}, x'_{lkd}]$. $\mathbf{T}_2$ is simply the selection matrix:

$$\mathbf{T}_2=\begin{bmatrix}1&0&0\\0&1&0\\0&1&0\end{bmatrix}. \tag{34}$$

The expression of ψ^r_{mqd} can be written as the following: $\psi^r_{mqd}=-\mathbf{X}_b\mathbf{i}^r_{qd0s}+\mathbf{A}_r\psi^r_{qdr}$, where $\mathbf{X}_b=diag[x_{bq},x_{bd},0]$ with $X_{bq}=(1/X_{mq}+1/X'_{lkq})^{-1}$ and $X_{bd}=(1/X_{md}+1/X'_{lfd}+1/X'_{lkd})^{-1}$:

$$\mathbf{A}_r=\begin{bmatrix}X_{bq}/X'_{lkq}&0&0\\0&X_{bd}/X'_{lfd}&X_{bd}/X'_{lkd}\\0&0&0\end{bmatrix}. \tag{35}$$

The dynamics of the mechanical subsystem can be written as

$$p\omega_r=\frac{\omega_b}{2H}(T_{pm}-T_e), \tag{36}$$

$$p\delta=\omega_r-\omega_e, \tag{37}$$

where $T_e=\psi^r_{ds}i^r_{qs}-\psi^r_{qs}i^r_{ds}$ and T_{pm} are the opposing electromagnetic torque and driven torque from the prime mover, respectively. Again, H denotes the rotor inertia (in seconds). The angle difference between the the synchronous reference frame and the rotor rotating frame is represented by δ. To transform the state variables from the rotor to synchronous reference frame, the transformation matrix ($^r\mathbf{K}^e$) can be applied to $\mathbf{f}^r_{qd0s}$. Due to the Hermitian property of this transformation matrix, the inverse transformation from the synchronous to rotor reference frame is just the transpose of $^r\mathbf{K}^e$:

$$^r\mathbf{K}^e=\begin{bmatrix}\cos\delta&\sin\delta&0\\-\sin\delta&\cos\delta&0\\0&0&1\end{bmatrix}. \tag{38}$$

A combustion engine, either a diesel engine or gas turbine depending on the size of the vessel, supplies the mechanical energy to the generator. The size of this combustion engine in the electric-driven ship is usually smaller than that in the direct mechanic-driven ship. For the purpose of examining the transient stability of the power generation unit in the large-scale vessel, a simplified model of a heavy-duty gas turbine is sufficient for this study. Based on the mathematical model of the single-shaft gas turbine in [30], the more simplified model, found in [26], is mainly composed of the speed governor (SG), valve positioner (VP), fuel system (FS), and turbine (T_{pm}). The state equation can be expressed as the following:

$$pSG=\frac{K_c}{T_c}\left(1-\frac{\omega_r}{\omega_b}\right)-\frac{K_c}{\omega_b}p\omega_r, \tag{39}$$

$$pVP=-\frac{1}{T_{FV}}VP+\frac{1}{T_{FV}}(SG+W_{F10s}), \tag{40}$$

$$pFS=-\frac{1}{T_{FT}}FS+\frac{1}{T_{FT}}VP, \tag{41}$$

where the torque supplied by the turbine shaft is given by the following relation:

$$T_{pm}=C_{1GT}(FS-C_{2GT})+C_{GNGT}\left(1-\frac{\omega_r}{\omega_b}\right).$$

All parameters of this model, given in Appendix II, are obtained from [26] to approximate the Allison 501 gas turbine.

Furthermore, the exciter/voltage regulator, controlling the field winding of the synchronous generator, is modeled according to a simplified model of the IEEE type 2 [31]. This type of exciter is typically accepted in the industry due to the model's simplicity. Three main components of this exciter are an independent power supply, a self-excited shunt field, and a stabilization feedback associated with gains and time constants. However, we neglect the nonlinear saturation in the shunt field. The state equations for

this type of exciter can be described as the following:

$$pV_R = -\frac{1}{T_A}V_R + \frac{K_A}{T_A}(V_{ref} - V_t - V_{stab}), \tag{42}$$

$$pE_{fd} = -\frac{K_E}{T_E}E_{fd} + \frac{1}{T_E}V_R, \tag{43}$$

$$pV_f = \frac{K_F}{T_{F1}}V_R - \frac{1}{T_{F1}}V_f, \tag{44}$$

$$pV_{stab} = -\frac{1}{T_{F2}}V_{stab} + \frac{1}{T_{F2}}\left(\frac{K_F}{T_{F1}}V_R - V_f\right). \tag{45}$$

All parameters of this exciter model are given in the per unit system in Appendix I. In this case, V_{ref} is fixed at a constant voltage of 1 p.u. and V_t is a magnitude of the generator's stator voltage. K_i and T_i, respectively, represent the gain and time constant corresponding to each subcomponent.

To connect electric machines together, a three-phase transmission line can be modeled as a symmetrical, three-phase, series RL circuit. This series RL circuit includes resistor ($\mathbf{r}_t$), self inductance ($\mathbf{L}_t$) from line leakage and magnetizing inductance, and mutual inductance ($\mathbf{M}_t$) from coupling of each line. The equations for the three-phase RL tie line in the $qd0$ synchronous reference frame are

$$p\mathbf{i}^e_{qd0t} = \mathbf{L}^{-1}_{qd0t}(\mathbf{v}_{qd0t} - \mathbf{r}_t\mathbf{i}^e_{qd0t} - \omega_e\mathbf{L}_{qd0t}\mathbf{T}_1\mathbf{i}^e_{qd0t}), \tag{46}$$

where $\mathbf{v}_{qd0t}$ represents the voltage difference between two different buses or machines.

Appendix B

Please see Tables 3–7.

Table 3
Parameters of the induction machines [26] in per unit with V_{base}=450 V.

Hp	r_s	X_{ls}	X_m	X'_{lr}	r'_r	H
200	0.01	0.0655	3.225	0.0655	0.0261	0.922
150	0.0051	0.00553	2.678	0.0553	0.0165	1.524

Table 4
Parameters of the 3.125 MW synchronous generator [26] in per unit with V_{base}=450 V.

r_s	r'_{kq}	r'_{fd}	r'_{kd}	X_{ls}	X'_{lkq}
0.00515	0.0613	0.00111	0.02397	0.8	0.3298
X'_{lfd}	X'_{lkd}	X_{mq}	X_{md}	H	
0.13683	0.33383	1.0	1.768	2.137	

Table 5
Parameters of the IEEE type 2 exciter/voltage regulator [31,26] in per unit.

T_R	V_{REF}	K_A	T_A	V_{RMAX}	V_{RMIN}
0	1	400	0.01	8.4	0
K_F	T_{F1}	T_{F2}	K_E	T_E	
0.01	0.15	0.06	1	0.1	

Table 6
Parameters of the simplified gas turbine with speed governor [26] in per unit.

K_c	T_c	T_{FV}	T_{FT}	W_{F10s}	C_{2GT}	C_{1GT}	C_{GNGT}
22.5	0.55	0.01	0.05	0.23	0.251	1.3523	0.5

Table 7
Parameters of the RL tie-line in per unit.

r_t	L_t	M_t
0.005	0.01	0.004

References

[1] Young S, Newell J, Little G. Beyond electric ship. Naval Engineers Journal 2001.
[2] Clayton DH, Sudhoff SD, Grater GF. Electric ship drive and power system. In: Conference rec. 2000, 24th international power modulation symposium. 2000. p. 85–8.
[3] Sudhoff SD, Kuhn BT, Zivi E, Delisle DE, Clayton D. Impact of pulsed power loads on naval power and propulsion systems. Electric ship research and development consortium (ESRDC) recent papers, nerc.aticorp.org/esrdc_recent_papers.html.
[4] Billinton R, Li W. Reliability assessment of electrical power systems using monte carlo methods. Springer; 2006.
[5] Schilling MT, Do Coutto Filho MB, da Silva AML, Billinton R, Allan RN. An integrated approach to power system reliability assessment. International Journal of Electrical Power and Energy Systems 1995;17:381–90.
[6] Hockenberry JR. Evaluation of uncertainty in dynamic, reduced-order power system models. PhD thesis, Massachusetts Institute of Technology, 2000.
[7] Hockenberry JR, Lesieutre BC. Evaluation of uncertainty in dynamic simulations of power system models: the probabilistic collocation method. IEEE Transactions on Power Systems 2004;19:1483–91.
[8] Ngamroo I, Dechanupaprittha S. Robust decentralized design of power system stabilizers taking into consideration system uncertainties. Optimal Control Applications and Methods 2005;26:35–53.
[9] Papaefthymiou G, Schavemaker PH, van der Sluisa L, Klinga WL, Kurowickac D, Cookec RM. Integration of stochastic generation in power systems. International Journal of Electrical Power and Energy Systems 2006;28:655–67.
[10] Stefopoulos GK, Meliopoulos AP, Cokkinides GJ. Probabilistic power flow with non-conforming electric loads. International Journal of Electrical Power and Energy Systems 2005;27:627–34.
[11] Helton JC, Oberkampf WL. Alternative representations of epistemic uncertainty. Reliability Engineering and System Safety 2004;85(1–3):1–10.
[12] Ghanem R, Spanos P. Stochastic finite elements: a spectral approach. New York: Springer-Verlag; 1991.
[13] Lucor D, Su CH, Karniadakis GE. Generalized polynomial chaos and random oscillators. International Journal of Numerical Methods in Engineering 2004;60:571–96.
[14] Wan X, Karniadakis GE. An adaptive multi-element generalized polynomial chaos method for stochastic differential equations. Journal of Computational Physics 2005;209:617–42.
[15] Xiu D, Karniadakis GE. The Wiener–Askey polynomial chaos for stochastic differential equations. SIAM Journal on Scientific Computing 2002;24:619–44.
[16] Xiu D, Lucor D, Su CH, Karniadakis GE. Stochastic modeling of flow–structure interactions using generalized polynomial chaos. Journal of Fluids Engineering 2002;124:51–9.
[17] Su Q, Strunz K. Stochastic circuit modelling with Hermite polynomial chaos. Electronics Letters 2005;41.
[18] Webster M, Tatang MA, McRae GJ. Application of the probabilistic collocation method for an uncertainty analysis of a simple ocean model. Technical report 4, Joint Program on the Science and Policy of Global Change, MIT, Cambridge, MA, 1996.
[19] Press WH, Teukolsky SA, Vetterling WT, Flannery BP. Numerical recipes in C, 2nd ed. Cambridge: University Press; 1992.
[20] Xiu D, Hesthaven JS. High-order collocation methods for differential equations with random input. SIAM Journal on Scientific Computing 2005;27:1118–1139.
[21] Petras K. Smolyak cubature of given polynomial degree with few nodes for increasing dimension. Numerische Mathematik 2003;93:729–753.
[22] Foo J, Wan X, Karniadakis GE. The multi-element probabilistic collocation method: error analysis and simulation. Journal of Computational Physics 2008;227:9572–95.
[23] Cameron RH, Martin WT. The orthogonal development of non-linear functionals in series of Fourier–Hermite functionals. Annals of Mathematics 1947;48:385–92.
[24] Gerstner T, Griebel M. Numerical integration using sparse grids. Numerical Algorithms 1998;18:209–32.
[25] Orszag SA, Bissonnette LR. Dynamical properties of truncated Wiener–Hermite expansions. Physics of Fluids 1967;10:2603–13.
[26] Mayer JS, Wasynczuk O. An efficient method of simulating stiffly connected power systems with stator and network transients included. Transactions on Power Systems 1991;6.

[27] Leon-Garcia A. Probability and random processes for electrical engineering, 2nd ed. Addison-Wesley; 1994.
[28] Karniadakis GE, Sherwin SJ. Spectral/hp element methods for CFD, 2nd ed. Oxford University Press; 2005.
[29] Krause PC, Wasynczuk O, Sudhoff SD. Analysis of electric machinery and drive systems, 2nd ed. New York: IEEE Press and Wiley-Interscience; 2002.
[30] Rowen WI. Simplified mathematical representations of heavy-duty gas turbines. Journal of Engineering for Power 1983;105:865–9.
[31] IEEE Committee Report, Computer Representation of Excitation Systems. IEEE Transactions on Power Apparatus and Systems 1968;PAS-87:1460–4.
[32] Wan X, Karniadakis GE. Multi-element generalized polynomial chaos for arbitrary probability measures. SIAM Journal on Scientific Computing 2006;28:901–28.
[33] Wan X, Karniadakis GE. Solving elliptic problems with non-Gaussian spatially-dependent random coefficients: algorithms, error analysis and applications. Computer Methods in Applied Mechanics and Engineering 2009;198:1985–95.
[34] Foo J, Karniadakis GE. Multi-element probabilistic collocation method in high dimensions. Journal of Computational Physics 2010;229:1536–57.
[35] Bieri M, Schwab C. Sparse high order FEM for elliptic sPDEs. Computer Methods in Applied Mechanics and Engineering 2009;198:1149–70.